



PCCP

Electron-induced vibrational excitation and dissociative electron attachment in methyl formate

Journal:	<i>Physical Chemistry Chemical Physics</i>
Manuscript ID	CP-ART-09-2019-005165.R1
Article Type:	Paper
Date Submitted by the Author:	27-Nov-2019
Complete List of Authors:	Kumar T P, Ragesh; J Heyrovsky Institute of Physical Chemistry Czech Academy of Sciences Kocisek, Jaroslav; J. Heyrovsky Institute of Physical Chemistry, Bravaya, Ksenia; Boston University, Chemistry Fedor, Juraj; J. Heyrovsky Institute of Physical Chemistry,

SCHOLARONE™
Manuscripts



Cite this: DOI: 10.1039/xxxxxxxxxx

Electron-induced vibrational excitation and dissociative electron attachment in methyl formate

Ragesh Kumar T P,^a J. Kočíšek,^a K. Bravaya^b and J. Fedor^aReceived Date
Accepted Date

DOI: 10.1039/xxxxxxxxxx

www.rsc.org/journalname

We probe the low-energy electron collisions with methyl formate HCOOCH₃, focusing on its resonant states. Experimentally, we (i) use the two-dimensional electron energy loss spectroscopy to gain the information about the vibrational excitation and (ii) report the absolute dissociative electron attachment cross sections. The electron scattering spectra reveal both the threshold effects due to the long-range electron-molecule interaction and a pronounced π^* resonance centered around 2.1 eV. This resonance gives rise to dissociative electron attachment into three different anionic channels, the strongest one being the production of the formate anion. Theoretically, we characterize this resonant state using the complex absorbing potential approach combined with multistate multireference perturbation theory, which predicts its position and width in an excellent agreement with the experiment.

1 Introduction

Electron collisions with methyl formate, HCOOCH₃, are interesting from the astrochemical point of view. This molecule has been detected in a number of outer space environments such as dense molecular clouds¹, molecular cores², or comets³. Its presence in these environments has inspired a large number of studies dedicated to elucidate its possible formation and destruction pathways^{4–9}. These were mainly focused on the neutral pathways and heterogeneous chemistry in ice cores, with one study of fragmentation induced by low-energy electrons.¹⁰

It is believed that in the interstellar space with low particle density, the decomposition reactions are to a large degree initiated by UV light, X-rays and cosmic rays (most of which are high-energy protons). When a high-energy radiation interacts with an interstellar icy grains that probably serve as reservoirs for chemical reactions, it produces an avalanche of secondary electrons - one high energy proton may release 10⁴ secondary electrons in its passage through a single ice-covered dust grain.¹¹ These secondary electrons have mean kinetic energies below 20 eV and may themselves trigger molecular decomposition. Three decomposition processes can be operative upon electron impact in this energy range: dissociation into neutral fragments, positive dissociative ionization and dissociative electron attachment (DEA). While the cross sections for the first two processes usually have thresholds in the 6 to 12 eV range and peak around 100 eV, the DEA process is resonant: it proceeds via formation of a transient negative ion

and commonly reaches very high cross sections at electron energies below 10 eV. It can thus represent an efficient decomposition process operative in the interstellar environment.¹² Recently, the DEA fragmentation pathways of methyl formate were reported qualitatively¹⁰ and a rich fragmentation pattern was found.

Methyl formate is an interesting target for electron collisions also from a purely fundamental point of view. The reason for it is that it is a methylated derivative of formic acid HCOOH. Resonant states and DEA mechanism in the latter have attracted a lot of attention, since two seemingly different mechanisms can play a role in its O-H bond cleavage induced by low-energy electrons: either a formation of π^* resonance associated with the double C=O bond,¹³ or the formation of a dipole-supported σ^* resonance associated with the O-H bond.¹⁴ The former mechanism requires breaking of the planar symmetry during the O-H dissociation and it has been suggested¹³ that it is the motion of the C-H bond (nondissociating hydrogen) which allows this dissociation. However, it has been shown experimentally, that the motion of the H atom has a very small (but observable) effect on the resulting cross section. Recently it has been suggested¹⁵ that this might be a purely academic dispute, since upon any breaking of the planar symmetry these two processes become indistinguishable. In any case, the vibrational excitation in formic acid is also intriguing:¹⁶ the π^* resonance is visible in all the vibrational excitation cross sections, apart from the actual O-H stretch, which shows only a broad threshold peak with narrow cusp structures.

In this respect, methylating the oxygen site and thus taking the methyl formate HCOOCH₃ as the target system, is potentially interesting from several reasons. The methyl group should shift the energy of the π^* resonance higher due to the inductive effect

^a J. Heyrovský Institute of Physical Chemistry v.v.i., Czech Academy of Sciences, Dolejškova 3, 18223 Prague 8, Czech Republic

^b Boston University, 590 Commonwealth Avenue, Boston, MA 02215, USA

known from the molecular orbital theory. At the same time, the dipole moment - a crucial factor in the σ^* (O-H) process - does not change much (1.42 D in formic acid, 1.77 D in methyl formate). And finally, since the whole methyl group is leaving instead of just an H-atom, the dynamical equilibrium is strongly shifted towards the electron autodetachment.

In the present paper, we experimentally probe the resonances in methylformate by means of electron energy loss spectroscopy and quantitative DEA spectroscopy. The computed resonance position and width support an assignment of the main resonance in the DEA cross-section to a π^* resonance.

2 Experiment

Three experimental setups were used.

The electron energy loss spectra were measured on the electrostatic spectrometer^{17,18} where the incident electron beam is produced by a hemispherical monochromator and the scattered electrons are analyzed by a hemispherical analyzer. All present experiments were recorded at a constant scattering angle of 135°. The elastic scattering cross section is brought to the absolute scale by comparison with the elastic scattering on helium, using the relative flow method as described in Ref 19. The error of absolute calibration is $\pm 20\%$. The vibrationally inelastic cross sections in methyl formate are calibrated with respect to its elastic cross sections by recording electron energy loss spectrum at constant incident energy and comparing the areas under the elastic and inelastic peak. Since the individual vibrations are not fully resolved, these vibrationally inelastic cross sections should be taken as indicative, we do not attempt to deconvolute the contributions from individual vibrations.

The dissociative electron attachment data are a combination of data taken on two different setups. First, the ion yield curves were recorded on a trochoidal DEA spectrometer with a quadrupole mass analyzer.^{20,21} Then, the absolute DEA cross sections were measured using the quantitative DEA spectrometer with a time-of-flight mass analyzer.^{22,23} The first quadrupole apparatus has better electron energy resolution (approx. 100 meV) than the second time-of-flight apparatus (approx. 250 meV), where the resolution is deteriorated by pickup of the high voltage pulsing signal. The final cross sections were obtained by scaling the quadrupole-setup ion yields to the time-of-flight setup absolute values using the invariance of the energy-integrated cross section. The electron energy scale and the absolute cross section were calibrated using the 4.4 eV resonance in O^- production from CO_2 . This resonance has a sharp onset at 3.99 eV and its shape has been measured with high energy resolution.²⁴ The calibration shift and the resolution are determined by convoluting the high-resolution spectrum²⁴ with a Gaussian of variable width and by fitting this width and energy shift to the current O^-/CO_2 data.

3 Complex absorbing potential calculations

The position and width of the π^* electronic resonance were computed using complex absorbing potential technique combined with extended multiconfigurational quasidegenerate perturbation theory of second order²⁵. cc-pVQZ valence basis was augmented

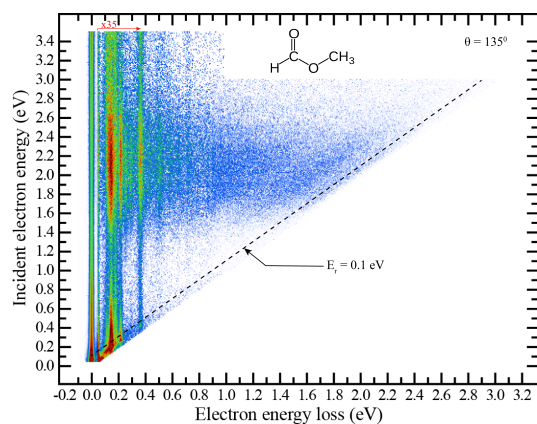


Fig. 1 Two dimensional electron energy loss spectrum of $HCOOCH_3$.

Table 1 Normal vibrational modes of methyl formate. The mode numbering, descriptions and optically measured frequencies are taken from Ref. 26.

Mode	Approximate description	Energy (meV)
v_1	CH_3 asymmetric stretching	378
v_2	CH_3 symmetric stretching	368
v_3	CH stretching	365
v_4	C=O stretching	217
v_5	CH_3 asymmetric bending	182
v_6	CH_3 symmetric bending	179
v_7	CH in plane bending	170
v_8	CH_3 in plane rocking	153
v_9	C-O stretching	150
v_{10}	H_3C-O stretching	115
v_{11}	OCO bending	95
v_{12}	COC bending	40
v_{13}	CH_3 asymmetric stretching	373
v_{14}	CH_3 asymmetric bending	180
v_{15}	CH_3 out of plane rocking	145
v_{16}	CH out of plane bending	128
v_{17}	COC out of plane bending (torsion)	-
v_{18}	CH_3-O torsion	-

with 3 even-tempered diffuse basis functions added to 6 ghost atoms located 1 Å above and below C_s plane at the positions of two oxygen atoms and carbonyl carbon atom (24 diffuse basis functions in total). The ghost atoms are fictitious charge-less atoms carrying basis functions. A p -type diffuse basis function with an exponent 1×10^{-9} was added to the basis set to mimic ionization. State-average CASSCF(5/11) calculation was performed with averaging over 12 states. The CAP onset along x, y , and z directions of 8 bohr was used for CAP-XMCQDPT2 calculation.

4 Results and discussion

4.1 Elastic scattering and vibrational excitation

Figure 1 shows the two-dimensional electron energy loss spectrum of methylformate recorded at the 135° scattering angle. The 2D spectrum provides a unified picture of the energy loss processes:^{27,28} the electron with the incident energy E_i (y-axis) has after the collision a smaller residual E_r and thus leaves its energy loss $\Delta E = E_i - E_r$ (x-axis) in form of the internal energy of the molecule. The vertical lines, clearly visible on the 2D spectrum, thus symbolize the excitation of individual vibrational modes (the strong line at $\Delta E = 0$ eV corresponds to the elastically scattered

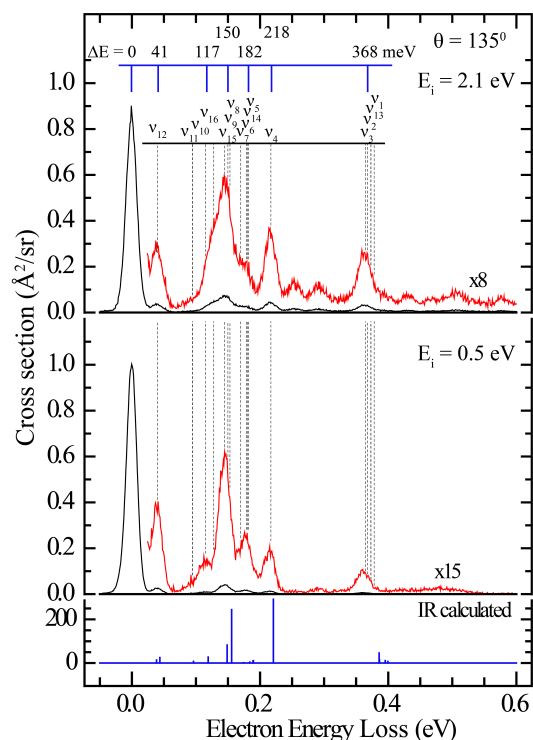


Fig. 2 Electron energy loss spectra of HCOOCH_3 recorded at two incident electron energies.

electrons). The intensity variations along these lines reflect the changes of the efficiency of vibrational excitation with the incident energy. Apart from vertical lines, a blurred signal across basically all energy losses - unspecific vibrational excitation - is visible in the incident energy range between 1.5 and 2.5 eV.

Figure 2 shows the electron energy loss spectra recorded at two different incident energies. They in principle correspond to the horizontal intensity cuts across the 2D spectrum along constant E_i values, however, they were recorded independently for improved signal-to-noise ratio. The vertical bars show the frequencies of methyl formate's normal modes from the optical IR spectroscopy.²⁶ The numbering of the modes follows the notation of Ref. 26. Table 1 lists the excitation energies and description of these modes. The electron impact vibrational excitation generally does not follow the optical selection rules and intensities, however, especially in non-resonant regions, it may be interesting to compare the excitation profile with the one expected based on the direct dipole excitation. We have thus calculated the expected IR intensities at MP2/aug-cc-pVTZ level, also shown in figure 2

Several remarks can be made about the excitation of various vibrational modes. At the incident energy $E_i = 0.5$ eV, the intensity profile actually closely follows the predicted IR intensities. This is not surprising: this incident energy lies close to the threshold for all these vibrations. Here, the mechanism of vibrational excitation is mainly due to long-range electron molecule interaction, mediated by the methyl formate's dipole moment. The dominant vibration is the C-O stretch ν_9 , other excited modes are the C-O-C bend ν_{12} , O-CH₃ stretch ν_{10} , C=O stretch ν_4 , and unresolved groups of CH bending (ν_5, ν_6, ν_7) and stretching (ν_1, ν_2, ν_3) modes.

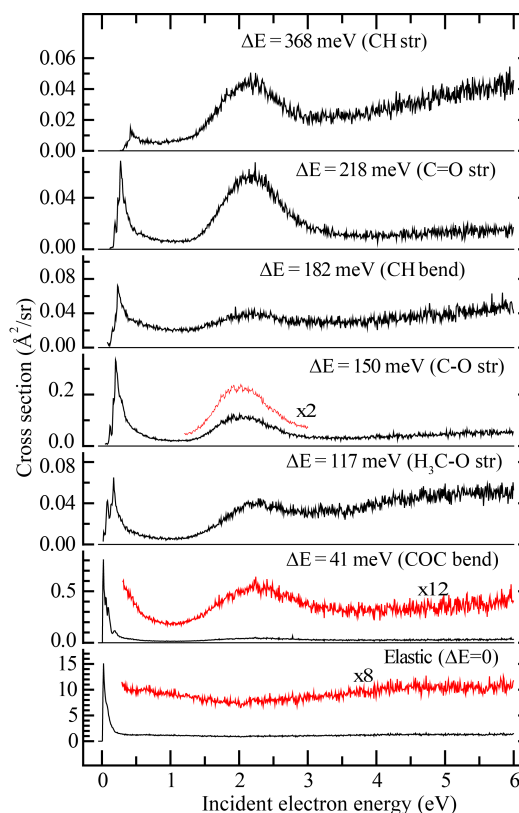


Fig. 3 Excitation curves of individual energy losses. The mode designations indicate the dominant vibration or group of vibrations contributing to this energy loss. The magnified part in the $\Delta = 150$ meV spectrum was recorded separately for better signal to noise ratio.

The situation is somewhat different in the resonance region. At the incident energy $E_i = 2.1$ eV, the dominant inelastic energy loss band is still the C-O stretch ν_9 . However, there is a clear relative increase of ν_4 , C=O stretch and the C-H stretching modes ν_1, ν_2, ν_3 . The ν_{10}, ν_9 and ν_5 peaks are much less resolved than in the non-resonant region, the resonance formation leads also to excitation of vibrations which lie between them: C-H out of plane bending ν_{16} and C-H in plane bending ν_7 . Also, the excitation of the overtones and combination vibrations is much more efficient at this incident energy. Their exact assignment is not possible, however, the progression of peaks visible between 0.2 and 0.4 eV has an approximate spacing of 40 meV from the ν_4 peak, it can thus be assigned to a combination of the C=O stretch and the O-C-O bend, $\nu_4 + n\nu_{12}, n = 1, 2$.

Figure 3 shows the excitation curves of individual energy losses, recorded at the positions marked in figure 2 by blue bars. In such a spectrum, the energy loss (= difference between the electron monochromator and analyser) is kept constant and the signal is recorded as a function of E_i . The spectra thus reflect the probability of excitation of the given energy loss. The individual panels are labeled by the dominant vibration contributing to this energy loss. The elastic scattering cross section, corresponding to zero energy loss, steeply rises at very low electron energies, a common effect in polar molecules.²⁹ Apart from this, the cross section shows a broad minimum around 2 eV. This decrease is

probably caused by the probability flux conservation - as seen below, at this energy the cross section for all the vibrational excitation channels rises, the number of elastically scattered electrons thus decreases.

The excitation curves for all the vibrational modes have similar shapes. Close to threshold, the excitation curve shows a pronounced peak. Again, such threshold peaks are common in all polar molecules.²⁹ Almost all present threshold peaks show a seeming structure, however, this is largely due to the fact that we do not fully resolve the individual vibrations. When a neighbouring vibration falls within the resolution of the spectrometer, its threshold peak will be visible in the excitation curve of the measured vibration, albeit at a different threshold, hence creating a secondary maximum in the recorded signal. This is unfortunate, especially from the point of view of the O-CH₃ stretching mode. In formic acid, HCOOH, the threshold peak of the O-H stretching vibration shows pronounced structures - vibrational Feshbach resonances - caused by the long-range molecule interaction. We cannot conclusively say, whether these structures are present also in the methyl formate.

The 2.1 eV resonance is visible in all the excitation curves. The C-O stretch excitation even shows a pronounced oscillatory structure superimposed on the resonance band. These are well known boomerang oscillations, created by the superposition of the outgoing and incoming nuclear wave packet. Again, the comparison with the formic acid case, where the π^* resonance was visible in all the excitations except for the O-H stretch, is complicated by the overlapping vibrations. There is a clear maximum in the excitation curve at $\Delta E = 117$ meV, but the spectrometer does not sample exclusively the O-CH₃ vibration.

We finally turn our attention to the unspecific vibrational excitation - the blurred signal visible in the center of the two-dimensional spectrum. It means, that in the incident energy range of the π^* shape resonance, a certain fraction of electrons is ejected with a continuous distribution of residual energies. Such an effect has been observed in a number of molecules³⁰ and is caused by the internal vibrational redistribution on the anion potential surface: upon formation of the resonance, the excess energy is randomized over the vibrational degrees of freedom and the electrons are emitted statistically.

Figure 4 shows the spectra of these electrons in detail. The top panel is the energy loss spectrum at a constant incident energy of $E_i = 2.1$ eV - a horizontal cut through the 2D spectrum (the same as in figure 2, here shown in the full energy loss scale). The electrons with an energy loss close to the incident energy of 2.1 eV are those emitted with near zero residual energies ($E_r = E_i - \Delta E$). The spectra are in principle similar to those observed in formic acid¹⁶ and a number of other molecules, with one notable difference. Usually, the abundance of statistical electrons shows a clear Boltzmann-like maximum at E_r close to zero. In figure 4a this would correspond to the peak at the complete energy loss of 2.1 eV. We see no such clear maximum, which may suggest electron detachment prior to the complete randomization of the excess energy.

The bottom panel of figure 4 shows the energy loss spectrum recorded at a constant residual energy of $E_r = 0.1$ eV. Such a

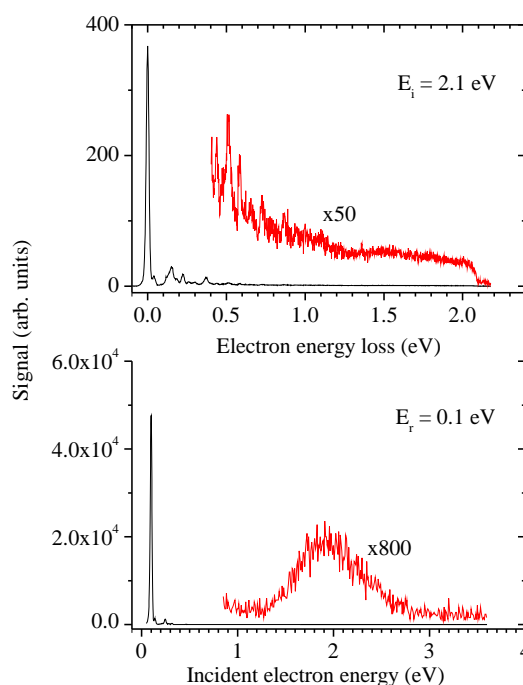


Fig. 4 Two spectra demonstrating the character of the unspecific vibrational excitation. Top panel: constant incident energy spectrum at $E_i = 2.1$ eV in the full energy loss scale. Bottom panel: energy loss spectrum recorded at constant residual energy of 0.1 eV.

spectrum in principle represents an intensity profile across the 2D spectrum along the diagonal marked in figure 1 and maps the abundance of threshold electrons as a function of the incident electron energy. This abundance clearly follows the entrance channel: formation of the 2.1 eV resonance.

4.2 Theoretical characterization of the resonance

The position and width of the π^* electronic resonance were computed using complex absorbing potential technique,³¹ combined with extended multiconfigurational quasidegenerate perturbation theory of second order perturbation theory [24]. CAP techniques allows one to extract the resonance position and width from a stationary point of the so-called η -trajectory, describing the

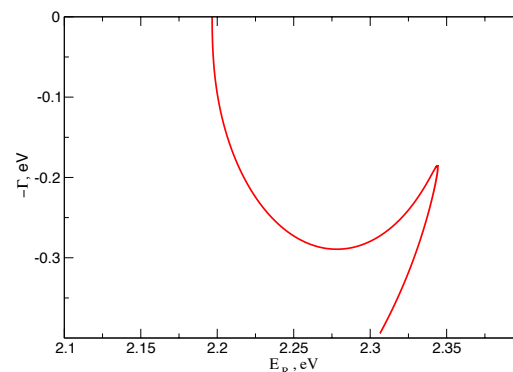


Fig. 5 CAP-XCMQDPT2/SA-12-CASSCF(5/11)/cc-pVQZ+6gh[3s] π^* resonance η -trajectory.

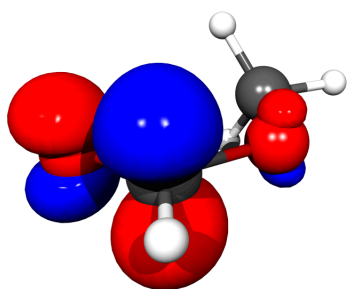


Fig. 6 SA-12-CASSCF(5/11) natural orbital predominantly singly occupied in the resonance state.

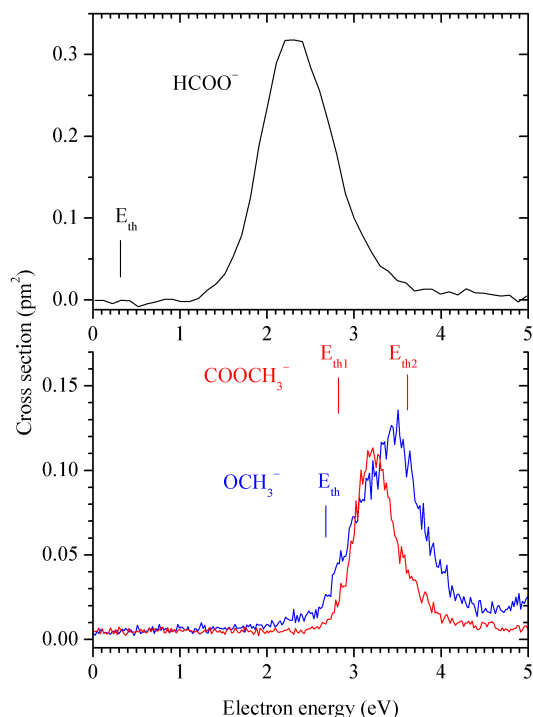


Fig. 7 Cross sections for dissociative electron attachment to HCOOCH_3 .

dependence of the complex eigenvalue of non-Hermitian CAP-augmented Hamiltonian on the CAP strength parameter η (Refs. 31,32 and refs. therein). The position and width of the resonance has been identified based on the minimum logarithmic velocity criterion.³¹ The trajectory exhibits a single stationary point associated with a cusp (Fig. 5) and allows one to unambiguously extract the estimates of the resonance position ($E_R=2.34$ eV) and electronic width (0.187 eV). Computed resonance position is in excellent agreement with the experiment.

The state is dominated by a configuration in which the π^* orbital (Fig. 6) is singly occupied. The actual scattering wavefunction lies in the continuum, however, the simplified picture of the 2.1 eV resonance as a temporal occupation of this orbital by the impinging electron sheds light in the experimental observations. The order of the bonds along which the orbital is antibonding will decrease upon the resonance formation, the potential energy gradient will thus induce the motion of nuclei in the directions

perpendicular of these nodal planes. The strong excitation of C-O stretch (ν_9) and C=O stretch (ν_4) vibrations is thus driven by this motion.

The strong excitation of the bending modes and the O-CH₃ stretch mode suggest an efficient breaking of the planar symmetry, which is necessary to make the anion potential surface dissociative in the direction of this mode. This will play a role in the DEA mechanism discussed below.

4.3 Dissociative electron attachment

Figure 7 shows partial cross sections for three DEA fragments: HCOO^- , resulting from the cleavage of the O-CH₃ bond, OCH_3^- , resulting from the cleavage of the C-O bond; and COOCH_3^- , resulting from the cleavage of one of the C-H bonds. The relative ion yield curves corresponding to these processes were recently reported by Feketeova et al.¹⁰ and are in excellent agreement with the present data. There are additional DEA bands above 5 eV electron energy. We do not discuss them here, since they are mediated by formation of core-excited resonances, which are not manifested in the electron scattering cross sections.

Table 2 Computed CCSD(T)/aug-cc-pVTZ threshold energies (eV) for formation of anionic fragments. The geometry optimization and frequency calculation was performed at MP2/aug-cc-pVTZ level of theory.

Dissociation channel	ΔE	$E_{th} = \Delta E + \Delta ZPE$
$\text{HCOOCH}_3 \rightarrow \text{HCOO}^- + \text{CH}_3$	0.64	0.30
$\text{HCOOCH}_3 \rightarrow \text{OCH}_3^- + \text{HCO}$	3.07	2.70
$\text{HCOOCH}_3 \rightarrow \text{COOCH}_3^- + \text{H}$	3.28	2.83
$\text{HCOOCH}_3 \rightarrow \text{HCOOCH}_2^- + \text{H}$	4.04	3.61

The vertical marks in figure 7 denote the positions of energetic thresholds obtained as the difference of total energies of the reactants and products including the zero point energies (ΔZPE). These are separately listed in table 2. For the COOCH_3^- fragment, the hydrogen can be cleaved from two sites: E_{th1} denotes the threshold for removing it from the C=O site, E_{th2} the threshold from removing it from the methyl group. The experimental signal clearly appears below the latter one and has a sharp onset at E_{th1} , we thus conclude that H-atom is cleaved from the C=O site. For the OCH_3^- fragment, the signal also appears at the threshold, but, interestingly, has a much shallower onset. Comparison with the vibrational excitation cross sections reveals the dissociation mechanism for these channels. The formation of the π^* resonance leads to nuclear motion both in the direction of stretching the C-O bond (ν_9) and stretching of the C-H bond (ν_3) - this is manifested by the efficient excitation of the corresponding vibrations. As soon as the available energy exceeds the dissociative threshold of a given bond, this initial nuclear motion leads to the dissociation of this bond.

The strongest DEA fragment HCOO^- has a surprisingly low threshold of $E_{th} = 0.3$ eV. However, the signal appears only at the region of the π^* resonance and copies the shape of the vibrational excitation cross sections. This means that the O-CH₃ bond cleavage is certainly mediated by the formation of this resonance. It is clearly not dissociative along merely stretching the O-CH₃

bond, the dissociation thus has to be accompanied by bending of the molecule. This is in accord with the strong excitation of bending modes and combination bands in the vibrational excitation at 2.1 eV.

The absence of anion formation at the predicted energetic threshold is in a way surprising from the point of view of the formic acid problem outlined in the introduction. In HCOOH, the HCOO⁻ anion is formed at its threshold. One of the two suggested DEA mechanisms - which received strong support from the experiments with partially deuterated formic acid³³ - is the dipole-supported σ^* resonance. The phrasing 'dipole supported' is crucial. In molecules without considerable long range interactions, σ^* resonances normally lead to very low DEA cross sections due to a small barrier towards electron detachment. The presence of a strong dipole moment (or even high polarizability in a non-polar molecule³⁴) can lead to the existence of a dipole-bound or virtual state in the scattering. The interaction of such a scattering state with the σ^* state causes a dramatic increase in the dissociative cross section. Such a cross section has then typically a sharp onset at the energetic threshold. Prototypical molecules where this mechanism is operative are hydrogen halides.^{35,36} The dipole moment of methyl formate (1.77 D) in principle opens this possibility, however, no measurable HCOO⁻ signal has been detected at the low energies around the threshold. It should be noted that the data from the Innsbruck group¹⁰ also do not show any signal at these energies. We estimate that if there is a DEA signal in methyl formate that originates from the dipole-supported σ^* (O-CH₃) mechanism, its cross section has to be at least 20 times weaker than for the mechanism originating from the π^* resonance.

A possible reason of the absence of this mechanism could be a dynamical effect: upon methylating the oxygen site, the competition between the electron detachment and dissociation moves strongly in the favor of the former - the experimental energy-integrated HCOO⁻ cross section in methyl formate is roughly 800 times smaller than that in the formic acid. The present findings could be explained if the cross section for the threshold mechanism was more sensitive to the mass of the dissociating fragment than the cross section for the π^* resonance mechanism. Indeed, the threshold dipole-supported mechanism shows very strong mass dependence. For example, the calculated cross section for hydrogen loss in formic acid drops by factor of 35 upon deuteration²⁹, methylation of the site can thus completely suppress the mechanism.

5 Conclusions

In conclusion, we probed the low-energy electron-induced chemistry in methyl formate with respect to its vibrational excitation and fragmentation via DEA. Both channels are dominated by the formation of a π^* resonance centered around 2.3 eV. The complex absorbing potential calculation reproduces the position of this resonance in an excellent agreement with the experiment. The strong excitation of the bending vibrations mediated by the resonance explains the occurrence of DEA fragmentation channels, that are symmetry forbidden without bending distortion of the molecular framework.

This work has been partly motivated by the dispute about the DEA mechanism of the dehydrogenation channel in formic acid HCOOH leading to HCOO⁻ production. The dissociative cross section in for the equivalent channel in methyl formate is approximately 800 times lower than in HCOOH. This is expected, since the methylation causes a strong shift of the dissociation-autodetachment competition in favor of the autodetachment. However, no DEA signal is observed close to its threshold, where one could in principle expect occurrence of the dipole-supported σ^* (O-CH₃) mechanism. A possible explanation for the lack of this signal could be its stronger dependence on the reduced mass of the dissociating system than for a π^* resonance-mediated mechanism.

Acknowledgments

This work has been supported by the Czech Science Foundation project 17-04844S and by the National Science Foundation (CHE-1665276 to K.B.B.). The authors thank R. Janečková for help with carrying out some experiments.

References

- 1 G. A. Blake, E. Sutton, C. Masson and T. Phillips, *Astrophysical Journal*, 1987, **315**, 621–645.
- 2 S. Cazaux, A. Tielens, C. Ceccarelli, A. Castets, V. Wakelam, E. Caux, B. Parise and D. Teyssier, *The Astrophysical Journal Letters*, 2003, **593**, L51.
- 3 D. Despois, N. Biver, D. Bockelée-Morvan and J. Crovisier, *Proceedings of the International Astronomical Union*, 2005, **1**, 469–478.
- 4 A. Horn, H. Møllendal, O. Sekiguchi, E. Uggerud, H. Roberts, E. Herbst, A. Viggiano and T. D. Fridgen, *The Astrophysical Journal*, 2004, **611**, 605.
- 5 P. A. Lawson, D. S. Osborne Jr and N. G. Adams, *The Journal of Physical Chemistry A*, 2012, **116**, 2880–2884.
- 6 C. J. Bennett and R. I. Kaiser, *The Astrophysical Journal*, 2007, **661**, 899.
- 7 G. Cui, F. Zhang and W. Fang, *The Journal of chemical physics*, 2010, **132**, 034306.
- 8 F. Fantuzzi, S. Pilling, A. Santos, L. Baptista, A. Rocha and H. Boechat-Roberly, *Monthly Notices of the Royal Astronomical Society*, 2011, **417**, 2631–2641.
- 9 J. S. Francisco, *Journal of the American Chemical Society*, 2003, **125**, 10475–10480.
- 10 L. Feketeová, A. Pelc, A. Ribar, S. E. Huber and S. Denifl, *Astron. Astrophys.*, 2018, **617**, A102.
- 11 S. Pimblott and J. la Verne, *Radiat. Phys. Chem.*, 2007, **76**, 1244–1247.
- 12 I. I. Fabrikant, S. Eden, N. J. Mason and J. Fedor, *Adv. At. Mol. Opt. Phys.*, 2017, **66**, 545–657.
- 13 T. N. Rescigno, C. S. Trevisan and A. E. Orel, *Phys. Rev. Lett.*, 2006, **96**, 213201.
- 14 G. A. Gallup, P. D. Burrow and I. I. Fabrikant, *Phys. Rev. A*, 2009, **79**, 042701.
- 15 M. Zawadzki, Čížek, K. Houfek, R. Čurík, M. Ferus, S. Civiš, J. Kočíšek and J. Fedor, *Phys. Rev. Lett.*, 2018, **121**, 143402.

- 16 M. Allan, *J. Phys. B*, 2007, **39**, 2939–2947.
- 17 M. Allan, *J. Phys. B*, 1992, **25**, 1559.
- 18 M. Allan, *J. Phys. B*, 2005, **38**, 3655.
- 19 M. Allan, *J. Phys. B*, 2007, **40**, 3531–3544.
- 20 M. Stepanović, Y. Pariat and M. Allan, *J. Chem. Phys.*, 1999, **110**, 11376.
- 21 J. Langer, M. Zawadzki, M. Fárnik, J. Pinkas, J. Fedor and J. Kočíšek, *Europ. Phys. J. D*, 2018, **72**, 112.
- 22 O. May, J. Fedor, B. C. Ibănescu and M. Allan, *Phys. Rev. A*, 2008, **77**, 040701(R).
- 23 O. May, J. Fedor and M. Allan, *Phys. Rev. A*, 2009, **80**, 012706.
- 24 R. Dressler and M. Allan, *Chem. Phys.*, 1985, **92**, 449.
- 25 A. Kunitsa, A. Granovsky and K. Bravaya, *J. Chem. Phys.*, 2017, **146**, 184107.
- 26 J. K. Wilmschurst, *J. Mol. Spectroscopy*, 1957, **1**, 201.
- 27 K. Regeta and M. Allan, *Phys. Rev. Lett.*, 2013, **110**, 203201.
- 28 M. Ranković, P. Nag, M. Zawadzki, L. Ballauf, J. Žabka, M. Polášek, J. Kočíšek and J. Fedor, *Phys. Rev. A*, 2018, **98**, 052708.
- 29 I. I. Fabrikant, *J. Phys. B*, 2016, **49**, 222005(1–20).
- 30 M. Allan, *J. Electron Spectrosc. Relat. Phenom.*, 1989, **48**, 219.
- 31 U. V. Riss and H.-D. Meyer, *J. Phys. B*, 1993, **26**, 4503–4536.
- 32 T. C. Jagau, K. B. Bravaya and A. I. Krylov, *Annu. Rev. Phys. Chem.*, 2017, **68**, 525–553.
- 33 R. Janečková, D. Kubala, O. May, J. Fedor and M. Allan, *Phys. Rev. Lett.*, 2013, **111**, 203201.
- 34 M. Allan, M. Lacko, P. Papp, Š. Matejčík, M. Zlatar, I. I. Fabrikant, J. Kočíšek and J. Fedor, *Phys. Chem. Chem. Phys.*, 2018, **20**, 11692.
- 35 M. Čížek, J. Horáček, A.-C. Sergenton, D. B. Popović, M. Allan, W. Domcke, T. Leininger and F. X. Gadea, *Phys. Rev. A*, 2001, **63**, 062710.
- 36 J. Fedor, C. Winstead, V. McKoy, M. Čížek, K. Houfek, P. Kolorenč and J. Horáček, *Phys. Rev. A*, 2010, **81**, 042702.